Journal of
Nanoscience and Nanotechnology
Vol. 5, 856–863, 2005

RESEARCH ARTICLE

Construction and 3-D Computer Modeling of Connector Arrays with Tetragonal to Decagonal Transition Induced by pRNA of phi29 DNA-Packaging Motor

YinYin Guo,[1] Forrest Blocker,[2] Feng Xiao,[1] and Peixuan Guo[1,*]

[1] *Department of Pathobiology and Wildon School of Bioengineering, Purdue University, West Lafayette, IN 47907, USA*
[2] *Institute for Cellular and Molecular Biology, School of Biological Sciences, University of Texas, Austin, TX 78712, USA*

The bottom-up assembly of patterned arrays is an exciting and important area in current nanotechnology. Arrays can be engineered to serve as components in chips for a virtually inexhaustible list of applications ranging from disease diagnosis to ultrahigh-density data storage. In attempting to achieve this goal, a number of methods to facilitate array design and production have been developed. Cloning and expression of the gene coding for the connector of the bacterial virus phi29 DNA-packaging motor, overproduction of the gene products, and the *in vitro* construction of large-scale carpet-like arrays composed of connector are described in this report. The stability of the arrays under various conditions, including varied pH, temperature and ionic strength, was tested. The addition of packaging RNA (pRNA) into the array caused a dramatic shift in array structure, and resulted in the conversion of tetragonal arrays into larger decagonal structures comprised of both protein and RNA. RNase digestion confirmed that the conformational shift was caused by pRNA, and that RNA was present in the decagons. As has been demonstrated in biomotors, conformational shift of motor components can generate force for motor motion. The conformational shift reported here can be utilized as a potential force-generating mechanism for the construction of nanomachines. Three-dimensional computer models of the constructed arrays were also produced using a variety of connector building blocks with or without the N- or C-terminal sequence, which is absent from the current published crystal structures. Both the connector array and the decagon are ideal candidates to be used as templates to build patterned suprastructures in nanotechnology.

Keywords: Bacteriophage phi29, pRNA, Connector, 3-D Computer Modeling, Rosette, DNA-Packaging Motor, Tetragonal Arrays, Decagonal Arrays.

1. INTRODUCTION

Of considerable interest in current nanotechnology is the synthesis of patterned arrays.[1–3] Such arrays can be used for a wide variety of applications. Recently, these lattices have been made of non-biological materials that are assembled to form layers. Various methods by which to assemble superlattices from ordered nanocrystals have been successful, including colloidal crystallization,[4] complementary interactions,[5–7] self-assembly of macromolecules,[7–9] and patterned etch pits.[10] However, in all of these methods, it is difficult to produce controlled structures. Biological lattices and arrays possess significant advantages over more traditional non-biological structures, since they are self-assembling and can more readily be connected directly with biological molecules.

Found in nature is an excellent, precision nano-material factory from which the materials for building superlattices can be harvested; cells. Cells manufacture a huge variety of nanomachines made of protein, DNA and RNA with atomic precision,[11] including motors,[8,12] arrays,[13] pumps, membrane cores, and valves. These bionanomachines can be

*Author to whom correspondence should be addressed.

 1533-4880/2005/5/856/008/$17.00+.25 doi:10.1166/jnn.2005.143

mimicked, extracted or incorporated into more traditional nanotechnology.[14–18] The list of potential applications for utilizing bionanotools in nanotechnology is extensive. For example, ordered biologically-based structural arrays could serve as templates for the further construction of superlattices and suprastructures.[8, 9]

Considerable success has been achieved in the production of DNA-based arrays. DNA-based arrays have a sturdy structure that may facilitate many potential uses.[19] Arrays from proteins and peptides have also been constructed.[1, 20, 21] Recently, our lab has also reported the use of RNA as a building block for the construction of nanoparticles and arrays.[7, 22]

There is one particularly attractive candidate found in the viral DNA-packaging machinery, from which both protein and RNA bionanocomponents may be harvested. The *Bacillus subtilis* bacteriophage phi29 DNA-packaging motor has three parts: the connector, a protein enzyme (gp16) and a ribonucleic acid (pRNA) (a 120-base phi29-encoded RNA).[23] These components can be combined *in vitro* to assemble a machine.[23, 24]

One of the important components of the viral DNA-packaging machinery is the connector. In different viruses, the individual portal proteins that comprise the connector share little sequence homology and exhibit large variations in molecular weight.[25] However, the possess a significant amount of morphological similarity.[26] In phi29, the connector is a dodecameric protein structure with a 36 Å central channel through which viral DNA is packaged into the capsid and exits during infection. In phi29 virtually all most every DNA molecule added can be efficiently packaged *in vitro*, with all components being overproduced and purified.[23, 24] The structure of the phi29 connectors has been determined at atomic resolution.[25, 44, 54] The connector ring consists of twelve α-helical subunits, with the central channel being formed by three long helices of each subunit. The ring is 138 Å across at its wide end, 66 Å at the narrow end, where the internal channel is 60 Å at the top and 36 Å at the bottom. The wider end of the connector is located in the capsid, and the narrow end partially protrudes out of the capsid. The connector is located at the five-fold vertex of the viral capsid, which leads to a symmetrical mismatch between capsid and portal.[27, 28] As previously assumed, such a mismatch is required for the smooth rotation of the portal protein during DNA packaging.[27, 55]

pRNA plays a novel and essential role in the packaging of DNA into procapsids (Fig. 1). Six copies of pRNA have been found to form a hexameric ring[28, 29, 56] which drives the DNA-packaging motor.[30, 31] "Hand-in-hand" interaction of the right and left interlocking loops can be manipulated to produce desired stable dimers, trimers, or hexamers of pRNA.[22, 28, 32] Computer models of the three-dimensional structure of pRNA monomer, dimer, and trimer have been constructed.[33]

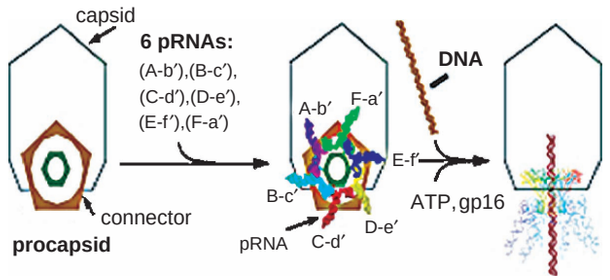

Fig. 1. Packaging of phi29 DNA through the motor with six pRNA A-b′, B-c′, C-d′, D-e′, E-f′, and F-a′.

This paper reports the conversion of the connector array from a tetrametric array of conical dodecagons to isolated decameric rosettes upon the addition of pRNA. Three-dimensional computer models for the arrays were also constructed. Both the connector array and the decagon are ideal candidates to be used as templates to build patterned suprastructures in nanotechnology.

2. MATERIALS AND METHODS

2.1. Cloning of the Gene Coding for the Connector

Wild-type phi29 DNA was purified from the virion by extraction at 70 °C for 15 minutes in TE buffer (50 mM Tris-HCl, pH 7.8/10 mM EDTA). The DNA was then digested with *Sna*BI (site 11303), *Sca*I (site 5192), and *Bst*NI (site 2742), resulting in fragments of 2742, 2450, 6111, and 7977 bp. The 6111-bp fragment containing the gene for gp10 was purified then cut with *Eco*Rl (site 9862), resulting in fragments of 4670 and 1441 bp. The 1441-bp *Eco*Rl/*Sna*Bl fragment, which contained parts of gene 10, was cloned into the *Eco*Rl/*Sma*l site of pBluescript (KS+), generating a plasmid pBlue10. The 4670-bp fragment, containing a part of gene 10, had an *Xho*I linker ligated to the Scal blunt end. The fragment was then cloned into pBluescript (KS+) at the *Eco*RI/*Xho*I site, generating a plasmid pBlue*Xho*l. A plasmid pBlue6K was constructed by combining two fragments from plasmids pBlue10 and pBlue*Xho*I. A 1441-bp *Eco*RI/*Bam*HI fragment was isolated from pBlue10 and ligated into the plasmid pBlue*Xho*I at the *Eco*RI/*Bam*HI sites. The *Nhe*I/*Bam*HI fragment (5643 bp) from plasmid pBlue6K was isolated and ligated to plasmid pARgp7[34] at the *Nhe*I/*Bam*HI sites, generating a plasmid pARgp7-8-8.5-10. To construct plasmid pAR10, the *Xba*I fragment was deleted from plasmid pARgp7-8-8.5-9-10.[34] The final map of plasmid pAR10 is displayed in Figure 2 panel I.

2.2. Purification of the Connector

An overnight culture (10 ml) of *E. coli* HMS174(DE3) containing plasmid pARgp10 was inoculated into 1 liter of LB broth with 50 μg/ml ampicillin and incubated at 37 °C

RESEARCH ARTICLE

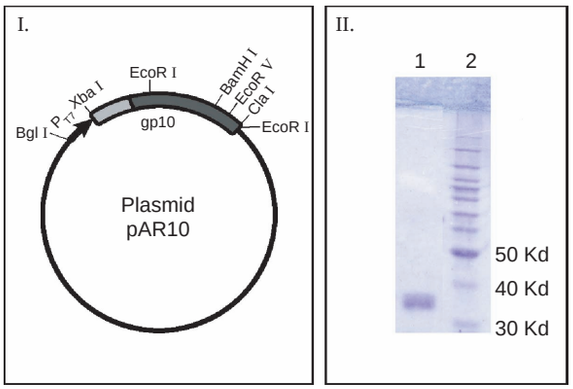

Fig. 2. (I) Map of the constructed plasmid for the expression of gp10, the connector protein subunit. (II) Coomassie blue staining of SDS polyacrylamide gel showing the purification of connector protein gp10 (lane 1) and the molecular weight marker (lane 2).

with vigorous shaking for 3 h. After adding isopropyl-beta-D-thiogalactopyranoside (IPTG) to a final concentration of 0.5 mM, the *E. coli* culture was incubated for an additional 3 h at 37 °C. Cells were pelleted at 5000 rpm at room temperature. The cell pellet was resuspended in 20 ml of Buffer A (50 mM Tris-HCL pH 7.7, 0.3 M KCl) and run through a French press twice at 10,000 psi. RNase (10 mg/ml) and DNase I (5 mg/ml) were added and the resulting solution was incubated at 4 °C for 1 hour. The cell debris was removed by centrifugation at 10,000 rpm in a JA20 motor (Beckman) for 2 h. The supernatant was loaded into a DE32 cellulose column (25×3 cm) equilibrated with buffer A, and the follow-through fraction was collected. The connector was further dialyzed against $1 \times$ Buffer B (0.1 M NaCl, 50 mM Tris-HCl pH 7.7, 5% glycerol) before running on P-11 phosphocellulose. After loading the sample to the P-11 column, the column was run with 4 volumes of buffer B containing 0.1 M NaCl and then with buffer B containing (1) 0.2 M NaCl; (2) 0.4 M NaCl; (3) 0.6 M NaCl; (4) 0.8 M NaCl. The connector was eluted by the gradient,[35] as revealed by SDS-PAGE. Ultracentrifugation and sucrose gradient sedimentation were further performed to concentrate the connector and remove the salt and other potential contaminants. The SDS-PAGE gel illustrating the purified protein is given in Figure 2 panel II.

2.3. Assembly of Arrays

Connector arrays were constructed using concentrated solutions of purified connector dodecamers. 3–4 mg/ml purified connector in 50 mM/Tris, pH 7.7, 0.6 M NaCl, and 5% glycerol was dialyzed against H_2O. The multilayer arrays were collected by centrifugation. A monolayer two-dimensional array was produced by treating the multilayer arrays with 2 M NaCl as has been described previously.[36]

2.4. 3D Computer Modeling of the Carpet Arrays

The crystal structure of a single dodecamer has been determined.[25] However, thirteen amino acids at the N-terminal and twenty six amino acids at the C-terminal of each gp10 subunit were missing from the published crystal structure of the connector.[25] Thus two different types of arrays, with or without N/C terminals, were constructed. Structural parameters and distance constraints of the connector reported in Ref. [25] were applied to the construction of the 3D model containing gp10 subunits without N- and C-terminal sequence (Fig. 4F, G). The coordinates of a quarter of the dodecamer (a trimer) (1H5W.pdb) were used as the basis for the construction of the array with N/C terminals. The amino acids absent from the coordinates in the trimer (gp10 chains A, B, and C) were added using the Deep View/Swiss-PDB Viewer program[37] (http://www.expasy.org/spdbv). Blast program was used to search for the model peptide templates that had the strongest similarity to the missing sequences as the first step in structure modeling. The N-terminal amino acids 1–15 were absent from all three gp10s and 16 was missing from subunit A and C of the trimer and 17 was also missing from C. These residues were added as an alpha helix in an orientation that would not conflict with the observed EM structure. Residues 166–169 were missing from B and C and were added in the orientation found in subunit A. The loop between alpha helix 5 and 6 was missing in all three chains: A-230-244; B-231-244; C-231-245. These were supplied as an alpha helix. Finally, the C-termini 285–309 were missing in all three chains and were supplied as an alpha helix oriented so as not to conflict with the EM structure. Each gp10 with extended coordinates was minimized using the molecular dynamics package NAMD[38] (http://www.ks.uiuc.edu/Research/namd). Minimization was performed for 200 steps using the Charmm force field (par_all27_prot_na.prm and top_all27_prot_na.top), in an explicit sphere of water. This structure was then replicated four times to form the dodecamer as the structure described.[25] Forming the dodecamper 3D carpet array using Deepview/Swiss-PDBViewer program[37] (http://www.expasy.org/spdbv). In this model, the subunit of each connector was arranged in an alternating up and down arrangement (Figs. 4, 5). Up and down layers of individual connector monomers were constructed to reflect distances observed in EM data. Once the distance from center to center of each monomer in both the up and down layers was fixed at 165 Å, the down layers were moved vertically so that several conditions were optimized: beta strand regions on the top and bottom of opposing up and down monomers were oriented to interface, while the alpha helical region in the interior was left to interface, the most neutral regions in the center of each opposing monomer were aligned, and the distance

RESEARCH ARTICLE

of closest approach for amino acids in the interior interface was minimized. The global position of the missing N- and C-terminal sequences was determined by pRNA binding assay, pRNA/protein crosslinking, protease cleavage, protein sequencing, and protein mutagenesis such protease cleavage after sequence insertion (Xiao and Guo, manuscript submitted for publication).

2.5. Conformational Shift Induced by pRNA

Phi29 pRNA of *Bacillus subtilis* bacteriophage phi29 was prepared as described previously.[39] Briefly, DNA oligomers were synthesized with the desired sequences and used to produce dsDNA by PCR. RNA was synthesized with the T7 promoter and then purified from a polyacrylamide gel. 5 μg arrays of connector (4 mg/ml) was mixed with 0.5 μg pRNA in TMS buffer (50 mM Tris-Cl (pH 7.8), 10 mM $MgCl_2$, 100 mM NaCl) for 5 to 10 minutes at room temperature. The complex was then loaded on 0.8% agarose gel in 1 $\times$ TAE buffer containing 10 mM $MgCl_2$, and the gel was run with constant current at 4 °C. The gel was first stained with ethidium bromide to show the presence of RNA bands, and then stained by Coomassie brilliant blue with gentle agitation at RT overnight to show the protein bands.

2.6. Electron Microscopy

Micrographs with negative staining were prepared by touching the 400-mesh grids covered with Formvarcarbon film for 1 second. The grids were then washed serially through 4 drops of 50 μl of distilled water, and then negatively stained with 1.5% aqueous uranyl acetate solution. After drying on filter paper, the sample grids were examined with a JEOL 100CX electron microscope.

3. RESULTS AND DISCUSSION

3.1. Cloning and Expression of the Gene Coding for Connector of phi29

A plasmid pARgp10 was constructed to carry the gp10 gene driven by a T7 promoter, and transformed into a host cell HMS174 (DE3). gp10 was overproduced after IPTG induction and the overproduced portal protein was analyzed by SDS Polyacrylamide Gel Electrophoresis (SDS-PAGE). A predominant band representing the gene product of the gp10 was found to agree with the predicted molecular weight of intact gp10, which is 35.8 kDa.[35]

3.2. Purification of Connector Protein and Construction of Carpet-Like Arrays

The over-expressed gp10 products were purified to homogeneity by ion exchange chromatography and sucrose gradient centrifugation.[40] The purified dodecamer connector protein can be assembled into a well-ordered carpet-like tetragonal array, as revealed by negative stained electronic microscopy (Fig. 4). Since the connector is a truncated cone, alternating face-up and face-down arrangements facilitated array formation (Figs. 4, 5). The multi-layer arrays were collected by centrifugation. A monolayer two-dimensional array was produced by treating the multilayer arrays with 1–2 M NaCl.[36]

3.3. Exhibited Stability of the Arrays Under Various Conditions

The minimum ion concentration requirement for connector array formation was determined through use of both polyacrylamide gel shift assay and sucrose gradient sedimentation. The arrays were tested using a procedure similar to that described in Ref. [22] and were found to be stable at pH values between 4 to 12, at temperatures

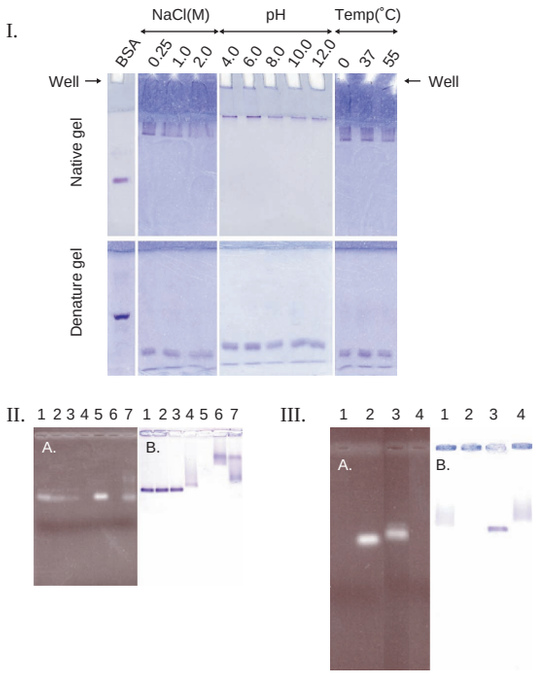

Fig. 3. (I) Native and denatured polyacrylamide gel showing the stability of the connector at different salt concentrations, pH values, and temperatures. (II) Agarose gel showing the interaction of phi29 motor pRNA with connector protein stained with ethidium bromide to show pRNA (A) and the same gel stained with Coomassie Blue to show the connector protein (B). (III) Agarose gel stained with ethidium bromide to show the pRNA (A) and the same gel stained with Coomassie Blue to show the connector protein (B) to evaluate the RNaseA digestion of the connector protein/pRNA complex.

Notes. (II) The purified connector (concentration 2.5 μg in μl of the final volume) was mixed with 0.5 μg (lane 1), 0.2 μg (lane 2), and 0.1 μg (lane 3) of phi29 motor pRNA. Lane 4, the purified connector alone; lane 5, pRNA alone; lane 6, tetragonal array alone; lane 7, tetragonal array plus pRNA. (III) Lane 1, the purified connector protein alone; lane 2, pRNA alone; lane 3, connector protein/pRNA complex; lane 4, connector protein/pRNA complex digested with RNaseA.

RESEARCH ARTICLE

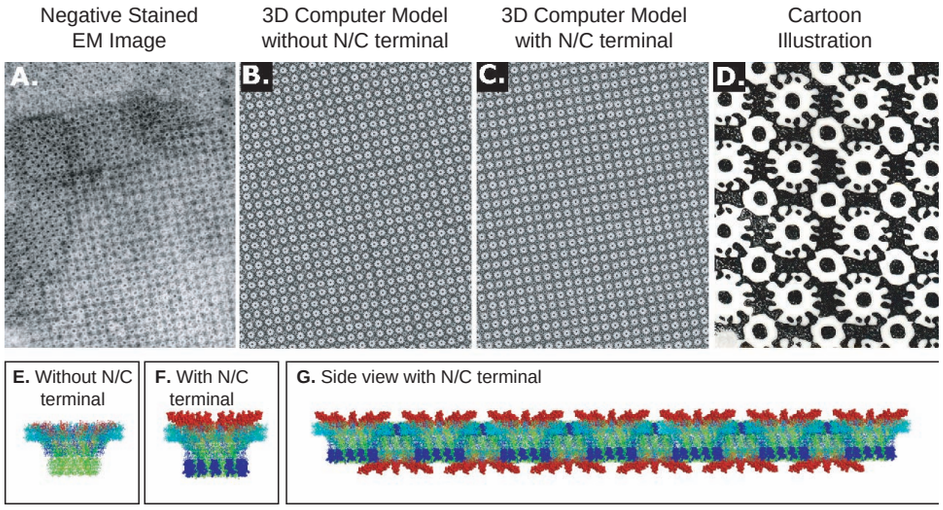

Fig. 4. Structure of the tetragonal arrays.

Notes. A. Negative-stained electron microscopy image of carpet array; B. Computer modeling without N/C terminal in black and white; C. Computer modeling with N/C terminal added in black and white; D. Drawing to elucidate the structure of carpet array of the tetragonal array; E. Side view of connector without N/C terminal; F. Side view of connector with N/C terminal added; G. Side view of 3D carpet array showing face-up and face-down arrangements. All computer models are in "ball & stick" representation. N terminal is represented in blue with space-fill representation. C terminal is represented in red with space-fill representation.

from −70 °C to 55 °C, and at salt concentrations as high as 2 M NaCl (Fig. 3, panel I). This indicated that the arrays were much more stable than individual protein subunits. Such stability can be credited to the tightly packed structure and to the intertwining interaction of the array molecules.

3.4. Computer Modeling of 3D Arrays

To elucidate potential applications of such arrays in nanotechnology, computer programs were used to construct 3D models. Using 3D coordinates of the crystal structure of the connector,[25, 41] a 3D array carpet was constructed and refined using the Deepview/Swiss-PDBViewer program. In this model, the subunit of each connector was arranged in an alternating up and down arrangement (Figs. 4, 5). The distance between each dodecamer was adjusted to 165 Å.

However, thirteen amino acids, 1-MARKRSNTYRSIN-13 at the N-terminal, and twenty six amino acids, 284-IVEQMRRELQQIENVSRGTSDGETNE-309 at the C-terminal, of gp10 were missing from the published crystal structure.[25] Based on our finding that this region was homologous to the corresponding flexible region in myosin,[42, 43] the inserted residues from 284 to 309 were treated as a flexible region needed for motor motion. In our computer model, all of these residues were added into the model, based on our recent finding that both the C-terminal and N-terminal residues, residues 1–13, were extended from the connector and that this region was the target for pRNA binding (Xiao et al., manuscript submitted for publication). Therefore, another type of model of arrays with N/C terminal were constructed (Figs. 4F, G).

In addition to the marked distinction between beta strand and alpha helical content in the top and bottom versus the center of each monomer, another notable feature of the model is the necessity for a 36 Å channel in the middle of the array. This channel is large and hydrophilic enough to accommodate a large amount of water (Fig. 5 Panel IV). On the top and bottom of the monomers, the spacing is close enough for van der Waals interaction. Since this portion of the monomer interface is dominated by beta strands, this suggests the possibility that the individual monomers might slide against one another. The computer model has been deposited into the PDB database with a deposit number of RCSB-3269 and corresponding pdb codes: 1YWE.pdb, 1VRI.pdb, and pbd.

3.5. Conformational Shift from Tetragonal Array to Decagonal Structure was Induced by the Addition of phi29 pRNA

When purified connector was mixed with pRNA and then subjected to 0.8% agarose gel electrophoresis, an extra band with slower migration rate appeared. This nascent band was stainable by both ethidium bromide (lane 1–3 in Fig. 3, panel II-A) and Coomassie brilliant blue (lane 1–3 in Fig. 3, panel II-B). The mixture was RNaseA sensitive (lane 4 in Fig. 3, panel III-A&B), suggesting the nascent band was the connector/pRNA complex. Also when the tetragonal carpet arrays were mixed with pRNA, there was also a nascent band which is sensitive to both ethidium

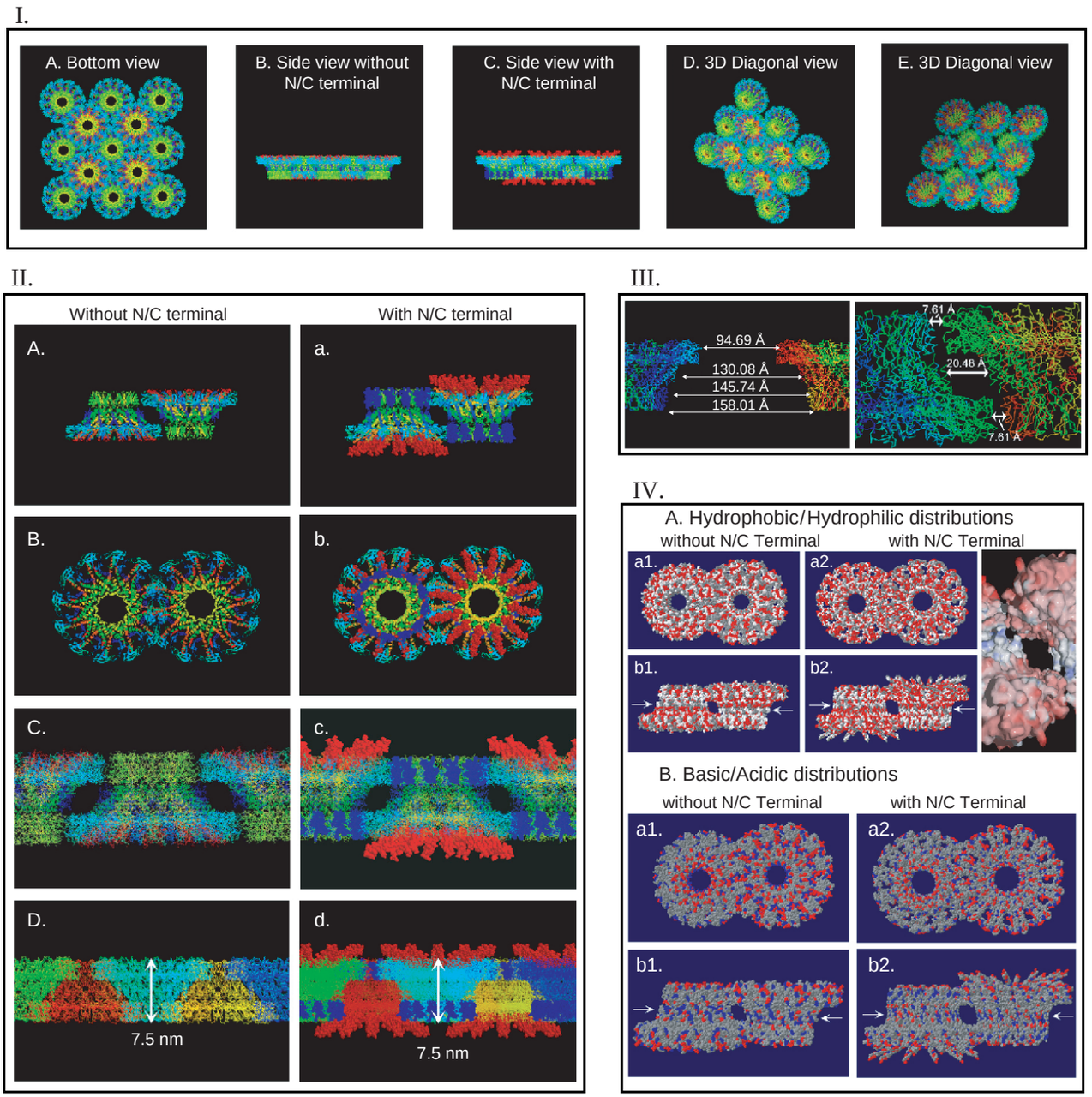

Fig. 5. (I) Birds-eye view of a 3 × 3 connector carpet array in wireframe representation viewed from different angles. (II) Side-by-side comparison of connectors without N/C terminal (A–D) on the left and with N/C terminals added (a–d) on the right. Side view and top view of the connector protein in ribbon representation. (III) Approximate distance between two adjacent upright connector proteins (A) and two proximal connector proteins with one upright and one downward (B), in backbone representation. (IV) Polar (A) and basic/acidic (B) distribution of two proximal connector proteins with one oriented upright and the other downward in space-fill representation viewed from the top (a1,a2) and from the side (b1,b2) and (c). Side-by-side comparison of connectors without N/C terminal (left) and with N/C terminal added (right).

Notes. (I) A. Bottom view; B. Side view without N/C terminal; C. Side view with N/C terminal added; D and E. Diagonal view. (II) A. Side view (A, C, D, a, c, d) and top view of two (A and B, a and b), three (C, c) and five (D, d) connector proteins, with docking of two connector proteins arranged with one up and one down from side view (A, a) and top view (B, b). Side view of the connector protein in wireframe representation with one line (C, c) and multiple lines in backbone representation (D, d). N terminal is represented in blue with space-fill representation. C terminal is represented in red with space-fill representation. (IV) In A, white color signifies hydrophilicity and red color the hydrophobicity. The two arrows in A–b1 and A–b2 point to a hydrophilic band in white (polar region). In A–c, a side-view orientation close-up is shown of one up and one down monomer interface. It illustrates that the top and bottom of each monomer are more negatively charged, whereas the interior interface is more neutrally charged and hydrophobic. In B, blue color signifies basic amino acids and the red color acidic amino acids.

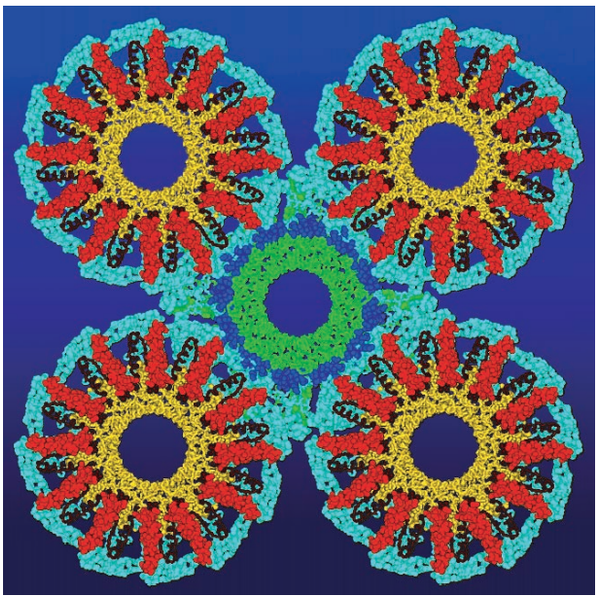

Fig. 6. Arrays with five connectors with complete sequence. One connector at the center is viewed from the narrow end, while four connectors at the corners of the square are viewed from the wide end.

bromide (lane 7 in Fig. 3, panel II-A) and Coomassie blue (lane 7 in Fig. 3, panel II-B). When pRNA was added to the carpet arrays, the array disappeared immediately, as revealed by negative stain electron microscopy (Fig. 6) and sucrose gradient sedimentation. The shift from tetragonal array to decagonal structure occurred when pRNAs were bound to the connector. The images of connectors and the decagon shown in Figure 6 reveal that the diameter of the decagon is larger than the connector, indicating that the change is not simply due to the elimination of two copies of the gp10 subunit from the connector after pRNA binding (Fig. 6). If this were the case, the decagon would be smaller than the connector.

As has been generally found in biomotors, the conformational shift of motor components generates force for motor motion.[40, 44–50] For example, it has been demonstrated that pRNA monomers possess two conformations, demonstrated by assessing the structure of pRNA in the presence or absence of Mg^{++} and other DNA-packaging components.[44] The conformation of pRNA in the presence and absence of Mg^{++} has been investigated with psoralen crosslinking,[44] nuclease probing,[44] and chemical modification.[51] The conformation of the pRNA bound to procapsids has been analyzed by RNase footprinting[52] and chemical probing.[53] The ability of pRNA to perform diverse functions despite being comprised of only four different building blocks (A, C, G, and U) can be attributed to its flexibility in conformational transition. Although the conformational shift reported here involves the connector protein, this shift can also be utilized as a potential force-generating mechanism for the construction of nanomachines.

One of the key steps in the integration of adapted biological components into nanotechnology is the bottom-up assembly of patterned arrays to be used as templates for the production of hybrids of biological, chemical, and other synthetic materials. The array reported here can be maintained when bio-moiety or chemical groups are added to the tetragonal or pentagonal structures. The stability of this array at a wide range of temperature and pH suggests the potential application for nanodevice. Once an effective bridge has been built between the biological templates and nanomachines, further applications will be possible. As noted earlier, patterned array structures could be important parts in nanotechnology. It is often necessary to generate force or to alter parts of the structure during computational, current shift, force shift, motor motion or force generation processes. The finding of a shift from tetragonal to decagonal structure that is induced by pRNA provides an interesting system for potential related applications. However, the specific applications of such processes need to be further elucidated and are currently under investigation.

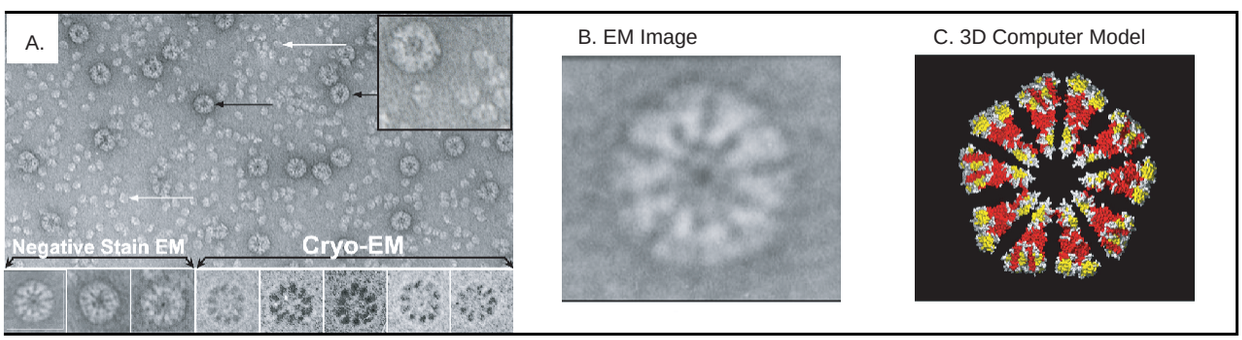

Fig. 7. Electron micrography showing conformational shift from tetragonal to decagonal array induced by pRNA.

Notes. Image was prepared after phi29 motor pRNA was added to the tetragonal carpet array. In (A), white arrows point to connectors, black arrows point to decagonal structures. Insert shows an enlargement of the size ratio between connector and rosette. (B) showing an enlarged image of a decagonal structure. (C) showing a computer model of the rosette.

Acknowledgments: We would like to thank Jeffrey Bolin for his insightful comments and assistance in the construction of computer model. We also acknowledge Dan Shu for technical assistance in gel preparation. In addition, we would like to thank Jeremy Hall for his assistance in the preparation of this manuscript. The research was supported by NIH grants R01-EB003730 from the Institute of Imaging and Bioengineering (program of NIH Nanoscience and Nanotechnology in Biology and Medicine). We appreciate Dr. Jose Carrascosa for his review and comments on 3-D construction of the connector.

References and Notes

1. D. Moll, C. Huber, B. Schlegel, D. Pun, U. B. Sleytr, and M. Sara, *Proc. Natl. Acad. Sci. USA* 99, 14646 (**2002**).
2. P. V. Braun, P. Osenar, and S. Stupp, *Nature* 380, 325 (**1996**).
3. Y. N. C. Chan, R. R. Schrock, and R. E. Cohen, *J. Am. Chem. Soc.* 114, 7295 (**1992**).
4. C. B. Murray, C. R. Kagan, and M. G. Bawendi, *Science* 270, 1335 (**1995**).
5. C. A. Mirkin, R. L. Letsinger, R. C. Mucic, and J. J. Storhoff, *Nature* 382, 607 (**1996**).
6. A. Paul Alivisatos et al., *Nature* 382, 609 (**1996**).
7. D. Shu, D. Moll, Z. Deng, C. Mao, and P. Guo, *Nano Lett.* 4, 1717 (**2004**).
8. D. Grigoriev, D. Moll, J. Hall, and P. Guo, *Encyclopedia of Nanoscience and Nanotechnology* 1, 361 (**2003**).
9. S. W. Lee, C. Mao, C. E. Flynn, and A. M. Belcher, *Science* 296, 892 (**2002**).
10. J. R. Heath, *J. Phys. Chem.* 100, 3144 (**1996**).
11. C. Zandonella, *Nature* 423, 10 (**2003**).
12. G. Oster and H. Wang, *Nature* 396, 279 (**2003**).
13. W. Shenton, D. Pum, U. B. Sleytr, and S. Mann, *Nature* 389, 585 (**1997**).
14. C. M. Niemeyer, *Trends Biotechnol.* 20, 395 (**2002**).
15. P. Hyman, R. Valluzzi, and E. Goldberg, *Proc. Natl. Acad. Sci. USA* 99, 8488 (**2002**).
16. S. Xiao, F. Liu, A. Rosen, J. F. Hainfeld, N. Seeman, K. Musier-Forsyth, and R. Kiehl, *J. Nanoparticle Res.* 4, 313 (**2002**).
17. R. K. Soong, G. D. Bachand, H. P. Neves, A. G. Olkhovets, H. G. Craighead, and C. D. Montemagno, *Science* 290, 1555 (**2000**).
18. H. Hess and V. Vogel, *Rev. Mol. Biotechn.* 82, 67 (**2001**).
19. C. Mao, W. Sun, and N. C. Seeman, *Nature* 386, 137 (**1997**).
20. H. Yan, S. H. Park, G. Finkelstein, J. H. Reif, and T. H. LaBean, *Science* 301, 1882 (**2003**).
21. P. Angenendt, J. Glokler, D. Murphy, H. Lehrach, and D. J. Cahill, *Anal. Biochem.* 309, 253 (**2002**).
22. D. Shu, L. Huang, S. Hoeprich, and P. Guo, *J. Nanosci. and Nanotech.* (*JNN*) 3, 295 (**2003**).
23. P. Guo, S. Erickson, and D. Anderson, *Science* 236, 690 (**1987**).
24. P. Guo, S. Erickson, W. Xu, N. Olson, T. S. Baker, and D. Anderson, *Virology* 183, 366 (**1991**).
25. A. Guasch, J. Pous, B. Ibarra, F. X. Gomis-Ruth, J. M. Valpuesta, N. Sousa, J. L. Carrascosa, and M. Coll, *J. Mol. Biol.* 315, 663 (**2002**).
26. C. Bazinet and J. King, *Ann. Rev. Microbiol.* 39, 109 (**1985**).
27. C. Chen and P. Guo, *J. Virol.* 71, 3864 (**1997**).
28. P. Guo, C. Zhang, C. Chen, M. Trottier, and K. Garver, *Mol. Cell.* 2, 149 (**1998**).
29. M. Trottier and P. Guo, *J. Virol.* 71, 487 (**1997**).
30. P. Guo, S. Grimes, and D. Anderson, *Proc. Natl. Acad. Sci. USA* 83, 3505 (**1986**).
31. C. Chen, S. Sheng, Z. Shao, and P. Guo, *J. Biol. Chem.* 275, 17510 (**2000**).
32. C. Chen, C. Zhang, and P. Guo, *RNA* 5, 805 (**1999**).
33. S. Hoeprich and P. Guo, *J. Biol. Chem.* 277, 20794 (**2002**).
34. C. S. Lee and P. Guo, *J. Virol.* 69, 5024 (**1995**).
35. C. Ibanez, J. A. Garcia, J. L. Carrascosa, and M. Salas, *Nucleic Acids Res.* 12, 2351 (**1984**).
36. J. M. Valpuesta and J. L. Carrascosa, *J. Mol. Biol.* 240, 281 (**1994**).
37. N. Guex and M. C. Peitsch, *Electrophoresis* 18, 2714 (**1997**).
38. L. Kale, R. Skeel, M. Bhandarkar, R. Brunner, A. Gursoy, N. Krawetz, J. Phillips, A. Shinozaki, K. Varadarajan, and K. Schulten, *J. Comput. Phys.* 151, 283 (**1999**).
39. C. L. Zhang, M. Trottier, and P. X. Guo, *Virology* 207, 442 (**1995**).
40. P. Guo, *Prog. in Nucl. Acid Res. & Mole. Biol.* 72, 415 (**2002**).
41. A. Guasch, A. Parraga, J. Pous, J. M. Valpuesta, J. L. Carrascosa, and M. Coll, *FEBS* 430, 283 (**1998**).
42. J. E. Walker, M. Saraste, M. J. Runswick, and N. J. Gay, *EMBO J.* 1, 945 (**1982**).
43. Y. Li, J. H. Brown, L. Reshetnikova, A. Blazsek, L. Farkas, L. Nyitray, and C. Cohen, *Nature* 424, 341 (**2003**).
44. C. Chen and P. Guo, *J. Virol.* 71, 495 (**1997**).
45. E. J. Mancini, D. E. Kainov, J. M. Grimes, R. Tuma, D. H. Bamford, and D. I. Stuart, *Cell* 118, 743 (**2004**).
46. M. Soncini, A. Redaelli, and F. M. Montevecchi, *J. Biomech.* 37, 1031 (**2004**).
47. K. Ito, T. Q. Uyeda, Y. Suzuki, K. Sutoh, and K. Yamamoto, *J. Biol. Chem.* 278, 31049 (**2003**).
48. M. Xiao, J. G. Reifenberger, A. L. Wells, C. Baldacchino, L. Q. Chen, P. Ge, H. L. Sweeney, and P. R. Selvin, *Nat. Struct. Biol.* 10, 402 (**2003**).
49. W. Liang and J. A. Spudich, *Proc. Natl. Acad. Sci. USA* 95, 12844 (**1998**).
50. P. D. Moens and C. G. dos Remedios, *Biochemistry* 36, 7353 (**1997**).
51. M. Trottier, Y. Mat-Arip, C. Zhang, C. Chen, S. Sheng, Z. Shao, and P. Guo, *RNA* 6, 1257 (**2000**).
52. R. J. D. Reid, J. W. Bodley, and D. Anderson, *J. Biol. Chem.* 269, 5157 (**1994**).
53. C. Zhang, M. Trottier, C. Chen, and P. Guo, *Virology* 281, 281 (**2001**).
54. A. A. Simpson, Y. Tao, P. G. Leiman, M. O. Badasso, Y. He, P. J. Jardine, N. H. Olson, M. C. Morais, S. Grimes, D. L. Anderson, T. S. Baker, and M. G. Rossmann, *Nature* 408, 745 (**2000**).
55. R. W. Hendrix, *Proc. Natl. Acad. Sci. USA* 75, 4779 (**1978**).
56. F. Zhang, S. Lemieux, X. Wu, S. St.-Arnaud, C. T. McMurray, F. Major, and D. Anderson, *Mol. Cell.* 2, 141 (**1998**).

Received: 13 December 2005. Revised/Accepted: 29 February 2005.